Impact of simplifications on numerical modelling of the shallow subsurface at city-scale and implications for shallow geothermal potential

N. Makasis[a,*], M.J. Kreitmair[a], A. Bidarmaghz[b], G.J. Farr[c], J.M. Scheidegger[d], R. Choudhary[a,e]

[a] *Department of Engineering, University of Cambridge, Trumpington Street, CB2 1PZ, UK*
[b] *School of Civil and Environmental Engineering, University of New South Wales, Sydney, Australia*
[c] *British Geological Survey, Cardiff University, Park Place, CF10 3AT, UK*
[d] *British Geological Survey, Environmental Science Centre, Keyworth, Nottingham NG12 5GG, UK*
[e] *Data-centric Engineering, Alan Turing Institute, UK*

[*] Corresponding author
Email address: nm735@cam.ac.uk (N. Makasis)

Preprint submitted to Science of the Total Environment *May 27, 2021*

Abstract

Anthropogenic infrastructures in the shallow subsurface, such as heated basements, tunnels or shallow geothermal systems, are known to increase ground temperatures, particularly in urban areas. Numerical modelling helps inform on the extent of thermal influence of such structures, and its potential uses. Realistic modelling of the subsurface is often computationally costly and requires large amounts of data which is often not readily available, necessitating the use of modelling simplifications. This work presents a case-study on the city centre of Cardiff, UK, for which high resolution data is available, and compares modelling results when three key modelling components (namely ground elevation, hydraulic gradient distribution and basement geometry) are implemented either 'realistically', *i.e.* with high resolution data, or 'simplified', utilising commonly accepted modelling assumptions. Results are presented at a point (local) scale and at a domain (aggregate) scale to investigate the impacts such simplifications have on model outputs for different purposes. Comparison to measured data at individual locations shows that the accuracy of temperature outputs from numerical models is largely insensitive to simplification of the hydraulic gradient distribution implemented, while changes in basement geometry affect accuracy of the mean temperature predicted at a point by as much as 3.5 °C. At the domain scale, ground temperatures within the first 20 m show a notable increase (approximately 1 °C volume-averaged and 0.5 °C surface-averaged), while the average heat flux over the domain is about 0.06 W/m^2 at 20 m depth. These increased temperatures result in beneficial conditions for shallow geothermal utilisation, producing drilling cost savings of around £1700 per typical household system or about 9% increase in thermal energy potential. Simplifications of basement geometry and (to a lesser degree) the hydraulics can result in an overestimation of these temperatures and therefore over-predict geothermal potential, while the elevation simplification showed little impact.

1. Introduction

Growing population sizes and the consequent requirements for infrastructures within urban areas are creating an increased demand on the shallow subsurface for competing uses, *e.g.* energy applications, transport networks, living spaces, and commercial structures. Infrastructures utilising the subsurface, such as ground heat exchangers (GHEs), tunnels, sewers, and structure basements, act as sources and sinks of heat within the ground and can lead to long-term and far-reaching thermal effects. The cumulative effect of these heat sources and sinks is a net-increase in underground temperatures, known as the Subsurface Urban Heat Island (SUHI). Increased subsurface temperatures can impact ventilation and cooling costs of underground spaces, efficiency of geo-energy systems, quality and quantity of groundwater flow, the health and maintenance of underground structures, and ecosystems [1–10], as well as goods production in underground spaces such as wine cellars [11]. It has been recommended that the use of increased shallow subsurface ground temperatures for energy generation could help mitigate negative impacts [12].

At the local scale, underground temperature increases due to anthropogenic heat fluxes into the ground are relatively well-established. In particular the effect of GHEs, such as energy piles or tunnels, on their immediate surroundings has been extensively reported [13–15]. Similar evidence exists for heated basements and their effects on the surrounding subsurface [16]. At a city scale, however, while the increase in general ground temperature due to urban infrastructure is acknowledged, less understanding exists of the magnitude of the variations in temperature across the larger area, as well as implications of such variation. A number of studies, experimental and numerical, indicate that impacts of anthropogenic heat flux into the shallow subsurface can be significant. A study in the city of Winnipeg, Canada, showed ground temperature anomalies caused by heat losses from buildings propagating as deep as 130 m below ground level [17], while another study at Turin, Italy, showed temperature increases at city scale, resulting chiefly from the operation of GHEs and ground-source heat pump systems (GSHP) [18]. However, the range of influencing features incorporated in these studies is limited, thereby potentially underestimating anthropogenic effects on the subsurface at city scale. Menberg *et al.* [19] concluded that the dominant factor in heat anomalies under the city of Karlsruhe, Germany, is the heat loss from basements, resulting in an appreciable increase in groundwater temperature beneath the city. Bidarmaghz *et al.* [20] showed increases in ground temperatures in the range of 1 to 5.5 °C within the Royal Borough of Kensington and Chelsea, London, due to the presence of subway tunnels and heated basements. Indeed, the operation of train lines worldwide have been shown to result in increased ground temperatures, impacting passengers' thermal comfort [21]. Rivera *et al.* [22] showed that raised urban ground temperatures in central Europe could reduce the GHE borehole length required for a given heating power supply by 4 m, while in some urban areas, the theoretical geothermal potential due to high subsurface temperatures beneath buildings is shown to exceed residential thermal demand [23]. Research has also been undertaken to develop models that can provide a more general understanding of the thermal state of the subsurface, such as a study at the city of Basel, Switzerland, focusing on groundwater resources [24]. Intensive deployment of shallow geothermal systems can impact groundwater systems at a neighbourhood scale [25] and, conversely, groundwater can play a key role in the long-term sustainability of shallow geothermal technologies, as identified by a study based in Germany [26]. The potential for using nested shallow geothermal systems in cities has also been shown by a recent study in Zaragoza, Spain [27], while a city-scale investigation for Vienna, Austria identifies key locations for improved utilisation of shallow geothermal energy [28]. At a larger scale, Ramos-Escudero *et al.* [29] have investigated shallow geothermal potential across Europe. With advances in shallow geothermal infrastructures, the use of energy geo-structures, such as energy tunnels, is another promising application for utilising the subsurface as thermal storage [30]. Ongoing and recent research on city-scale subsurface thermal effects in recent years, whilst encouraging, is still nascent. There remain a number of unknowns with respect to key features of the shallow subsurface and their impact on ground temperatures. Furthermore, there is no consensus across the community regarding the salient features of models necessary for accurate representation and interpretation of model outcomes.

The lack of detailed knowledge on the effect of anthropogenic influences on the subsurface at city scale is in part a consequence of limited availability of long-term subsurface temperature data [31], resulting in the need for accurate numerical simulations to model the relevant interactions over extended periods of time. However, numerical modelling of the subsurface at such scales introduces further challenges such as the high computational complexities and requirements of running large-scale simulations. Moreover, uncertainty around thermal-hydrological phenomena and subsurface heterogeneity, amongst other factors, create significant constraints on developing meaningful and representative models [2]. The scarcity of relevant data is an issue present in a number of studies modelling the subsurface, often resulting in the need to employ modelling simplifications (in combination with reducing computational complexity), such as of feature geometry (*e.g.* basements) or of the modelling of hydrology, to name but a few [1, 9, 32–39]. In particular, one aspect that has not been subject to extensive investigation is the impact of surface elevation at city-scale modelling, as in most cases a flat surface is assumed for simplicity. Understanding the impact of such simplifications on the realism of the model output under different conditions is crucial for effective and accurate modelling of the subsurface (including computational savings where appropriate).

In this paper, an analysis of modelling simplifications with respect to their impact on modelling accuracy (in terms of temperatures predicted) is presented through a case-study on the city centre of Cardiff, UK, expanding on an initial study presented in [40]. This study area was chosen in collaboration with the British Geological Survey (BGS), due to the availability of associated data from 'Cardiff Urban Geo Observatory' project [41], a city scale project focused on understanding urban groundwater systems. The data include detailed hydrogeological information, time series groundwater temperatures [42, 43], a 3D geological model [44], a hydrogeological model, and a high-resolution representation of buildings containing heated basements. These data are provided by the British Geological Survey (BGS). This study is unique and novel because it leverages the availability of detailed subsurface information to examine the model complexity necessary for yielding reasonably accurate outputs. In doing so, this study outlines scenario-based instances where simplifications may be employed and, depending on the scale of output considered, the magnitude of impact resulting from such simplifications. The paper is structured as follows. Section 2 outlines the numerical model framework, adapted from the semi-3D approach developed by Bidarmaghz *et al.* [20, 45] and introduces the simplifications considered in this paper, typical for such models, namely simplifications to elevation implementation, hydraulic head distribution, and basement geometry. Acknowledging that city-scale modelling is used to simulate scenarios across a range of different size scales and conditions, Section 3 explores results at both a local point-based scale and a global domain-based scale, highlighting how simplifications affect results obtained in the context of different modelling purposes. Computational times are reported to gain an understanding on potential savings and further help inform the provided modelling choice suggestions. Finally, conclusions as to the suitability of different modelling simplifications in different contexts are drawn in Section 4.

2. Methodology

This work utilises a numerical methodology that models the subsurface when subjected to anthropogenic heat sources at a city scale. This methodology further incorporates the modelling of the River Taff that crosses this modelled area, the systematic modelling of elevation levels, realistic hydraulic head distributions throughout the domain, and detailed material properties based on measured data. This section details the study area selected to undertake relevant analyses, namely the city centre of Cardiff in Wales, UK, followed by a detailed description of the numerical modelling implementation as well as an explanation of the modelling simplifications that are investigated.

2.1. Study area

The city centre of Cardiff, UK (Figure 1), is selected as study area to model and examine the impact of modelling choices on temperature outputs. The location is chosen due to the availability of 1) hydraulic head and 3D geological data [44] from a detailed hydrogeological model of the region, and 2) a large number of temperature time-series measurements [43] from monitoring boreholes within the area, taken over the course of several years, courtesy of BGS and Cardiff Harbour Authority. The monitoring boreholes are located throughout the city and measure temperature at various depths in the shallow subsurface. The existing knowledge and data for this area reduce the uncertainties that are commonly present for such large-scale modelling and allow for a focused study on the impact of modelling features. Moreover, the modelled area is selected in an attempt to balance available data and computational expense, while retaining a relevant mixture of basement types and geological features within the model domain. The study area consists of a rectangle of about 3.5 km^2 in the Southeast part of the city, shown in Figure 1b.

Hydrogeology of study area

The city of Cardiff is located on the south coast of Wales, United Kingdom, on the coast of the Bristol Channel (see Figure 1). Lithologic characteristics of the modelled domain are determined from data provided by the BGS, comprising of the lithologic classification within a 50 m $\times$ 50 m grid for a number of depth values up to 45 m below ground level. The raster grid is used to generate a linearly interpolated function of the thermal and hydraulic properties to be used by the finite element solver as shown in Figure 2a. Values of these properties are given in Table 1.

For locations with unavailable data regarding the local lithology, best-guess values based on the available literature are used, as indicated in the table.

Figure 1: Location of study area [46] and outlines of buildings with heated basements. © Crown copyright and database rights 2021 Ordnance Survey [100021290 EUL]. Use of this data is subject to terms and conditions.

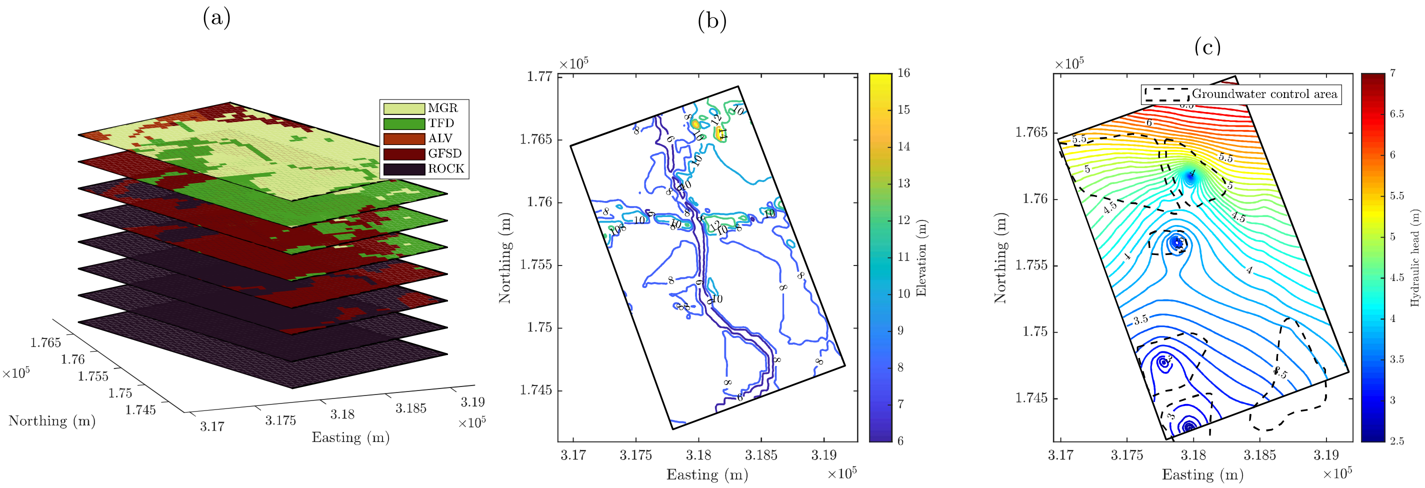

Figure 2: Geological distribution (panel a), elevation contours (b), and hydraulic head distribution (c) within study domain. Groundwater levels are pumped within dashed regions (copyright BGS, UKRI). © Crown copyright and database rights 2021 Ordnance Survey [100021290 EUL]. Use of this data is subject to terms and conditions.

Table 1: Thermal and hydraulic properties of geological materials present in the modelled domain and concrete material used for heat sources. Thermal diffusivity was calculated according to $\alpha = \lambda/(\rho C_p)$. Where appropriate, top values in a row represent partially saturated conditions and bottom values fully saturated conditions [47–51].

Geology/ Material	Average depth range [m]	Thermal conductivity, λ [W/(m K)]	Density, ρ [Mg m^{-3}]	Specific heat capacity, C_p [kJ/(kg K)]	Porosity, ε [-]	Hydraulic conductivity, k_h [m/s]	Thermal diffusivity, α [m^2/s]
Made ground, MGR	0 - 2.31	1.00 2.00	1.80	1.27	0.35	2.31×10^{-5}	4.37×10^{-7} 8.75×10^{-7}
Alluvium, ALV	0.76 - 2.66	1.40 2.40	1.67	1.18	0.35	1.00×10^{-5}	7.10×10^{-7} 1.21×10^{-6}
Tidal flat deposits, TFD	2.01 - 6.72	1.2 1.50	1.67	1.18	0.2	1.00×10^{-8}	6.09×10^{-7} 7.61×10^{-7}
Glacio-fluvial sediment deposits, GFSD	4.98 - 10.86	0.50 1.80	2.00	1.75	0.2	2.50×10^{-3}	1.43×10^{-7} 5.14×10^{-7}
Bedrock (Mercia Mudstone), ROCK	10.86 - 45	1.10 1.80	2.01 2.10	0.80	0.25	1.00×10^{-7}	6.84×10^{-7} 1.07×10^{-6}
Concrete	N/A	1.80	2.30	0.88	N/A	N/A	8.89×10^{-7}

The upper-most layer of the area studied consists predominantly of made ground (man-made deposits on the natural ground surface, MGR) underlain by tidal flat deposits (TFD), glaciofluvial sand and gravel deposits (GFSD) and alluvium (ALV). The tidal flat deposits confine the glaciofluvial sand and gravel aquifer in the southern part of the city. The Quaternary sequence is underlain by low permeability Triassic aged Mercia Mudstone bedrock (ROCK), which is considered to be base of the glaciofluvial sand and gravel aquifer. Below a depth of approximately $z = -25$ m, the domain consists almost exclusively of the Mercia Mudstone bedrock. The surface elevation of the area based on ground level measurements provided by the BGS are shown in Figure 2b, giving a difference of about 13 m from highest to lowest point within the model domain.

A hydraulic head distribution is generated from a detailed hydrogeological model developed by the BGS, shown in Figure 2c. In several regions of the city, the groundwater levels are artificially controlled to mitigate the rise in groundwater levels, particularly in areas with a large number of basements, resulting in a more complex distribution [52]. The difference in hydraulic head within the region is relatively small, resulting in a shallow hydraulic head gradient of approximately 1.6×10^{-3}. The groundwater level is found to be on average 4 m below the surface, varying depending on the surface elevation.

Heat sources within study area

The primary sources of anthropogenic thermal fluxes to the ground considered in this work are heated basements. In reality, depending on the location, other heat sources are also present in the underground, *e.g.* sewage networks, electrical cable tunnels, culverted watercourses, different types of ground-source heating and cooling schemes and historic landfill sites, the inclusion of which can increase the computational cost of a numerical model. The focus of this study remains on the heated basements as the dominant source of anthropogenic influence, given the local conditions and limitations on available information. For example, little information is available on the presence of ground-source heat pump systems, as there is no requirement to register closed-loop heat pump systems with local authorities.

Basement geometries were estimated from building footprints, obtained from Ordnance Survey 'Master Map', used under licence to BGS [53]. Footprints for buildings within the domain were reviewed according to their attributes (residential, commercial, or industrial use etc.) as well as local knowledge, to develop an understanding of the likelihood of each building having a heated basement, resulting in the distribution shown in Figure 1. Basements are assumed to extend into the ground a total depth of 3 m and to be constructed using concrete. In the model, the basement temperature are raised to $T_{\text{room}} = 18$ °C over a period of 30 days using a sigmoid function and then maintained at this temperature. This basement temperature gives outputs in good general agreement with measured temperatures and aligns with values reported in literature [8, 9, 35, 45, 54].

2.2. Numerical modelling

For the numerical modelling performed in this work a semi-3D approach is used, developed by Bidarmaghz *et al.* [45]. This methodology allows for the modelling of large areas and has been validated numerically against more complex full 3D methodology which, in turn, has been validated both experimentally and numerically [13, 45, 55]. The model is expanded to include additional features needed for this study. Simulations were run for a period of 20 years in total, to allow for effects such as thermal accumulation to manifest sufficiently.

Governing equations

The adopted numerical modelling methodology sub-divides the 3D geometry of the domain into a set of coupled 2D horizontal planes. Within planes, heat flow is modelled through conduction in porous media and convection via groundwater flow. Planes are thermally coupled to their nearest neighbours by out-of-plane heat fluxes. This semi-3D approach is illustrated in Figure 3, showing an example collection of planes, each defined at a different depth.

The equations governing the ground temperature, T_g (°C), within a plane are that of convective and conductive heat transfer [56] (incorporating groundwater flow), expressed as:

$$(\rho C_p)_{\text{eff}} \frac{\partial T_g}{\partial t} + \rho_f C_{p,f} \mathbf{v}_f \nabla T_g + \nabla \cdot \mathbf{q} = \mathbf{0}, \tag{1}$$

where ρ_{eff} is the effective density (kg/m^3), $C_{p,\text{eff}}$ the effective specific heat capacity (J/(kg K)), t is time (s), ρ_f is the fluid (groundwater) density (kg/m^3), $C_{p,f}$ is the specific heat capacity of the fluid, $\mathbf{v_f}$ is the Darcy velocity of the fluid (m/s), and $\mathbf{q}$ is the heat flux (W/m^2). The heat flux is related to the gradient of the ground temperature field via the effective thermal conductivity, *i.e.* $\mathbf{q} = \lambda_{\text{eff}} \nabla T_g$, where the effective thermal conductivity is given by $\lambda_{eff} = (1-\varepsilon)\lambda_m + \varepsilon\lambda_f$, where λ_m and λ_f are the thermal conductivity (W/(m K)) of the porous solid and of the groundwater, respectively, and ε is the porosity (-) of the ground. Other effective ground properties are calculated in the same manner.

Within each layer, the single-phase fluid flow through a porous medium is modelled using Darcy's Law, which relates the Darcy velocity field of the fluid to the total head gradient ∇Z and the dynamic viscosity of the fluid μ_f (Pa s) and the properties of the porous medium,

$$\mathbf{v}_f = -\frac{K}{\mu_f} \left(\nabla p_f - \rho_f \mathbf{g} \nabla Z \right), \tag{2}$$

where the permeability K (m^2) of the material is related to the hydraulic conductivity k_h (m/s) by $K/\mu_f = k_h/(\rho_f \mathbf{g})$. Combining equation (2) with the continuity equation, $\nabla \cdot (\rho_f \mathbf{v}_f) = 0$, gives the generalised governing equation, *i.e.*

$$\nabla \cdot \rho_f \left[-\frac{K}{\mu_f} \left(\nabla p_f - \rho_f \mathbf{g} \nabla Z \right) \right] = 0. \tag{3}$$

Equations (2) and (3) are solved for the Darcy velocity and the fluid pressure and coupled to (1) through this velocity.

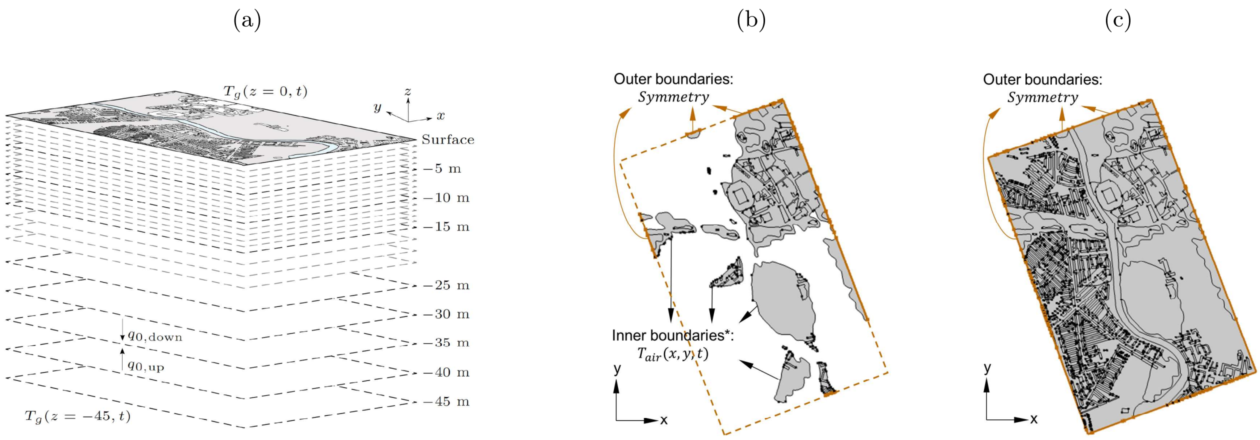

Figure 3: Schematic of the modelling approach, showing the collection of 2D planes interconnected by heat flux transfer and the temperature boundary conditions at the top and bottom planes. The lateral boundary conditions are shown on the right.

*Note that plot (b) is only applicable for realistic elevation modelling (explained in section 2.3), in layers where only some domains are modelled due to their elevation

Inter-plane heat transfer is taken into account by setting up out-of-plane heat fluxes. Defining the distance between the planes as d_z (m), equation (1) is altered to take into account sources of heat flux from planes above and below through inclusion of source terms:

$$\mathrm{d}_z(\rho C_p)_{\mathrm{eff}}\frac{\partial T_g}{\partial t} + \mathrm{d}_z\rho_f C_{p,f}\mathbf{v}_f\nabla T_g + \nabla\cdot\mathbf{q} = q_{0,\mathrm{up}} + q_{0,\mathrm{down}}, \tag{4}$$

where the upside and downside out-of-plane heat fluxes for plane n, respectively, are given by

$$q_{0,\mathrm{up}} = \lambda_{\mathrm{eff}}\left(T_{n-1} - T_n\right)/\mathrm{d}_z, \tag{5}$$

and

$$q_{0,\mathrm{down}} = \lambda_{\mathrm{eff}}\left(T_{n+1} - T_n\right)/\mathrm{d}_z. \tag{6}$$

The river flow is modelled using incompressible (water) turbulent single-phase flow physics, and coupled to the heat transfer physics in terms of temperature, pressure and velocity. The Reynolds-averaged Navier-Stokes (RANS) equations are implemented for conservation of momentum as well as the continuity equation for conservation of mass, as seen in Equations 7 and 8 respectively. Equations 9 and 10 present the transport equations for the turbulent kinetic energy, k, and the turbulent dissipation rate, ϵ, respectively. Lastly, Equations 11, 12 and 13 further define factors of the previous equations. These governing equations for turbulent flow are solved for the pressure and velocity vectors of the fluid flowing within the river which are then coupled to the heat transfer equations to calculate the transfer of heat and thus distribution of temperature within the domain.

$$\rho_f(\boldsymbol{u_f} \cdot \nabla)\boldsymbol{u_f} = \nabla \cdot [-p_f \boldsymbol{I} + \boldsymbol{K}] + \boldsymbol{F}, \tag{7}$$

$$\rho \nabla \cdot \boldsymbol{u_f} = 0, \tag{8}$$

$$\rho(\boldsymbol{u_f} \cdot \nabla)k = \nabla \cdot \left[(\mu + \frac{\mu_T}{\sigma_k}\nabla_k\right] + P_k - \rho_f \epsilon, \tag{9}$$

$$\rho(\boldsymbol{u_f} \cdot \nabla)\epsilon = \nabla \cdot \left[(\mu + \frac{\mu_T}{\sigma_\epsilon}\nabla_\epsilon\right] + \frac{C_{\epsilon 1}\epsilon}{k}P_k - \frac{C_{\epsilon 2}\rho_f \epsilon^2}{k}, \tag{10}$$

$$\boldsymbol{K} = (\mu + \mu_T)(\nabla \boldsymbol{u_f} + (\nabla \boldsymbol{u_f})^T), \tag{11}$$

$$\mu_T = \frac{\rho_f C_\mu (k)^2}{\epsilon}, \tag{12}$$

$$P_k = \mu_T \left[\nabla \boldsymbol{u_f} : (\nabla \boldsymbol{u_f} + (\boldsymbol{u_f})^T)\right], \tag{13}$$

where ρ_f is the density of water (kg/m^3), u_f is the velocity vector for the water (m/s), p_f is the pressure of water (Pa), I the identity matrix (-), μ the dynamic viscosity of water (Pa $\cdot$ s), μ_T the eddy or turbulent viscosity (m^2/s), k is the turbulent kinetic energy (m^2/s^2), F is the volume force vector (N/m^3), ϵ is the turbulent dissipation rate (m^2/s^3) and the empirically calculated coefficients σ_k, $\sigma\epsilon$, $C_{\epsilon 1}$, $C_{\epsilon 2}$, C_μ have values of: 1, 1.3, 1.44, 1.92, 0.09 respectively (as per [57]).

Boundary and initial conditions

The initial and boundary conditions applied to the model allow the governing equations to be solved for the relevant variables, in this case temperature, velocity and pressure. These conditions constitute knowledge applied to the model, such as the value of these variables at specific times or locations. The boundary and initial conditions applied in the model are:

- An initial temperature profile given by (14) at $t = 0$ is applied throughout the modelled domain.

- Basements constituting heat sources, as outlined in Section 2.3, are initiated at the same temperature as the ground and, over a period of 30 days, raised to and then maintained at 18 °C.

- At the upper-most plane, a time-varying heat flux into the layer from above is applied by (5) with T_{n-1} set to the value given by (14).

- At the bottom-most plane, a heat flux into the layer from below is determined by (6) with $T_{n+1} = T_{0,\ g}$ =12.9 °C [42].

- At the lateral boundaries of each plane, a symmetry boundary condition is applied, unless a realistic surface elevation is modelled, in which case a temperature boundary condition equal to the surface temperature is applied at the inner boundaries of contour domains above the ground, as shown in Figure 3.

- Hydraulic head values are assigned throughout the domain using the specified distribution, depending on the modelling simplification, explained in Section 2.3.

- The temperature of the water entering the river domain is defined by $10.98 + 5.107 \sin\big(\omega t + 2.134\big)$, where $\omega = {}^{2\pi}/_{365}$ rad/day, fitted to available measurement data for the river Taff provided by Cardiff Harbour Authority.

- A fluid velocity of 3 m/s is assigned at the inlet of the river based on measurements along the River Taff provided by the Cardiff Harbour Authority.

Undisturbed ground temperature

Taking into account the seasonal temperature fluctuation in the air as well as the geological features, the undisturbed ground temperature as a function of time and depth (including the temperature applied at the top of the model representing the ground surface) is approximated using a combination of semi-empirical models presented by Beardsmore and Cull [58] and Baggs [59] as:

$$T_g(z,t) = T_{0,g} - 1.07 k_v T_{amp} e^{-\epsilon z} \cos\left[\omega(t - t_0) - \epsilon z\right], \tag{14}$$

where $T_{0,g}$ is the mean annual ground temperature (°C), T_{amp} the seasonal heating cycle amplitude (°C), $\omega = {}^{2\pi}/_{P}$ is the angular frequency of the heating cycle (rad) with period $P = 365$ days, $\epsilon = \sqrt{{}^{\pi}/_{(P\alpha)}}$, α is the thermal diffusivity of the ground (m^2/s), k_v is the vegetation coefficient (defined spatially based on the surface cover conditions, adopting a value of 0.9 for suburban and 1.0 for urban terrain [60]), and t_0 is the day of coldest temperature after January 1st. From deep borehole measurements [42], the mean annual ground temperature is determined to be $T_{0,g} = 12.9$°C. The values of $T_{amp} = 6.5$°C and $t_0 = 26$ days are adopted, determined from weather data from the Cardiff area [61].

2.3. Modelling simplifications

This paper focuses on the impact modelling choices and simplifications can have on the accuracy of results obtained from numerical modelling of heat transfer in the shallow underground. Three key modelling choices are considered: hydraulic head distribution, resolution of surface elevation, and resolution of basement geometry. These are key modelling factors for which detailed information is often not available, or which may be exceedingly complex to implement realistically and, consequently, frequently simplified in modelling of the subsurface. To examine the impacts these simplifications may have, a realistic and a simplified version for each factor is implemented, resulting in eight different modelling combinations constituting eight different models. The realistic and simplified representations of these choices are shown in Figure 4. The following nomenclature is adopted to distinguish models: $E_iH_jB_k$, where 'E' denotes elevation, 'H' hydraulic distribution, and 'B' basement geometry and subscripts may be either 'R', indicating realistic implementation of the relevant factor, or 'S', for simplified modelling. For example, the model named $E_SH_RB_R$ implements a simplified elevation (Figure 4d), a realistic hydraulic head distribution (Figure 4b), and a realistic basement geometry (Figure 4c). Other parameters potentially affecting temperature values obtained, such as material properties, surface and initial ground temperature parameters, or basement distribution and temperature, are held the same across all implementations for the purposes of this work and will be investigated in detail in further work.

The realistic elevation implemented in the model, shown in Figure 4a, is generated using LIDAR data (OS Terrain® 50) (Figure 2b) and aggregating the surface values to averaged contours of 3 m increments resulting in the domains. In contrast, the simplified elevation approach utilises a flat model where only the base of the river is placed at 2 m below the surface. The hydraulic head distribution is provided from a detailed hydraulic model produced by BGS, as explained in section 2.1, and the simplified distribution is created using the average values along the north and south boundaries of the domain and assuming a uniform gradient between them. The basement footprints are obtained as outlined in Section 2.1 and the simplification is undertaken such that the total basement area is kept equal between the two and the locations of the simplified basements are close to the realistic ones, while keeping the assumed simplified footprint. It is worth noting that the Principality Stadium (located just east of the river) is not modelled as having heated basements, based on local knowledge. While the modelling is specific to the Cardiff case

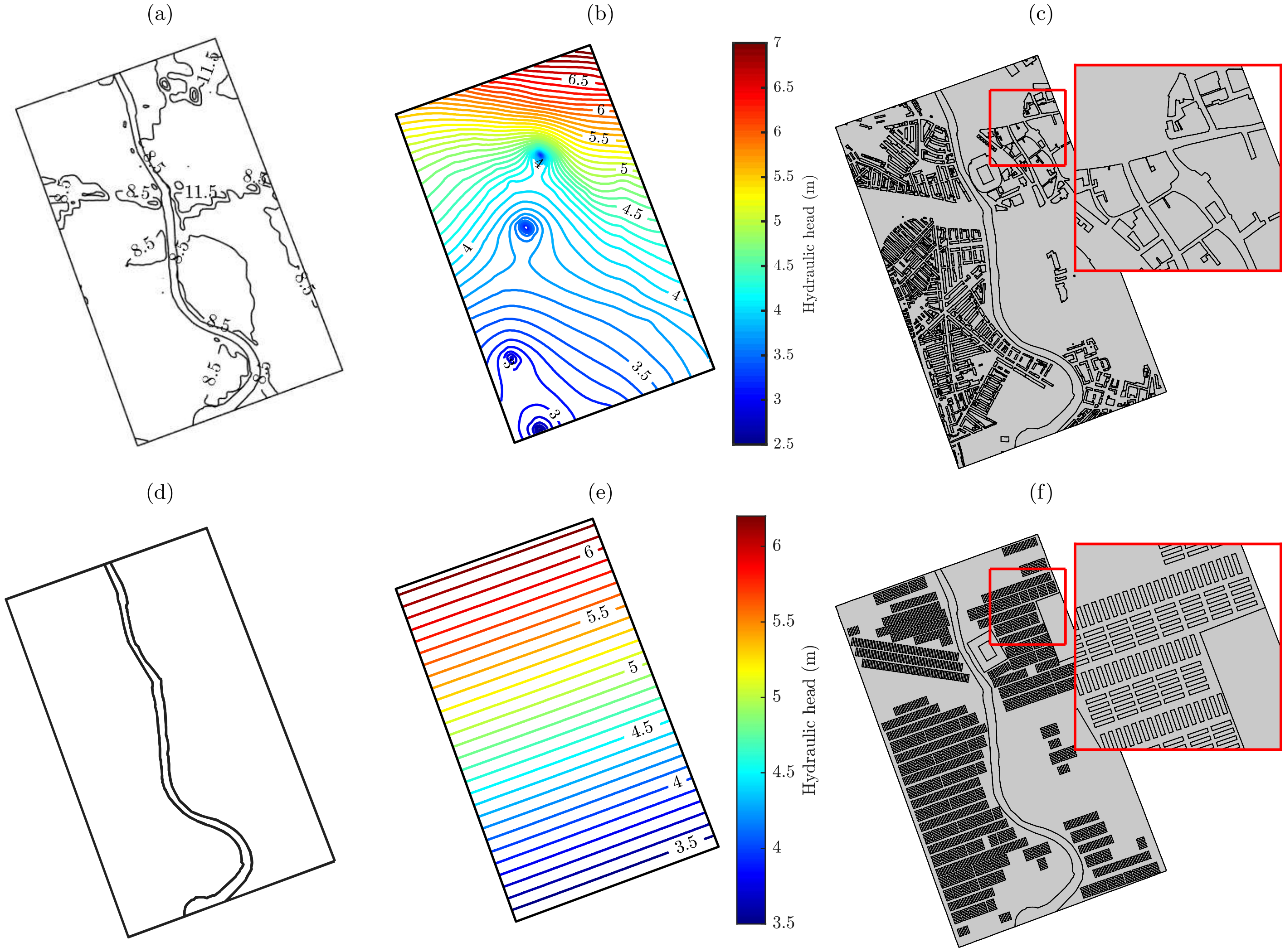

Figure 4: Modelling simplifications: showing how Elevation (panels (a) and (d)), Hydraulic distribution (panels (b) and (e)) and the basement geometry (panels (c) and (f)) are modelled either realistically (top row) or simplified (bottom row). © Crown copyright and database rights 2021 Ordnance Survey [100021290 EUL]. Use of this data is subject to terms and conditions.

study area, insights can nonetheless be generalised to other sites as to the conclusions drawn regarding the significance of realism in these modelling choices.

3. Results

An example of typical output from the numerical models is shown in Figure 5 for model combination $E_S H_R B_R$, illustrating the volume of data generated, visualised in different ways.

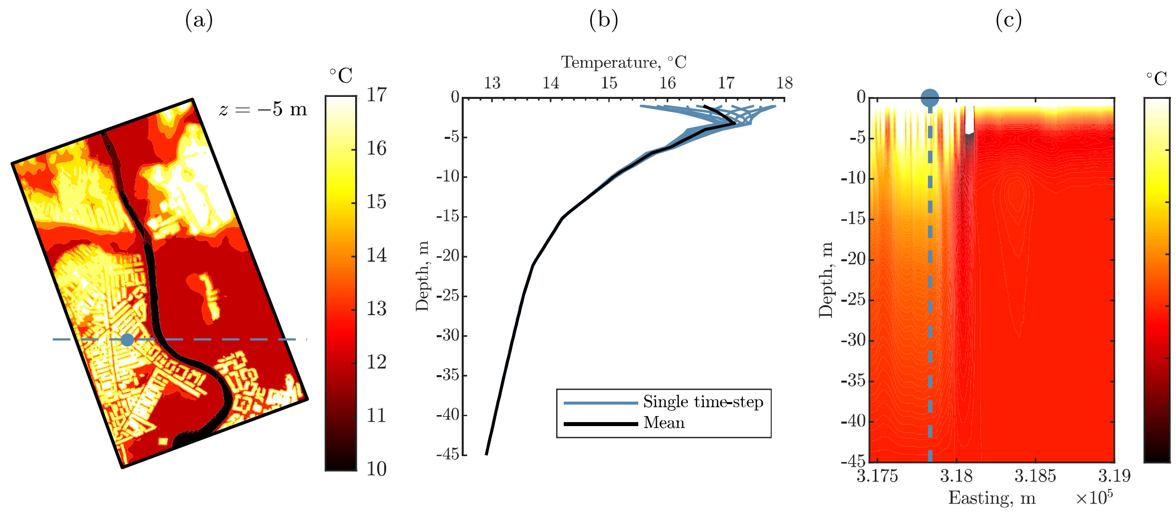

Figure 5: Typical model outputs from $E_S H_R B_R$ (i.e. model with simplified (flat) elevation, realistic hydraulic head distribution, and realistic basement footprints implemented : temperature distribution within domain at a depth of 5 m below ground level (panel a), average domain temperature profile (b), and a vertical slice temperature distribution at the location indicated (c). Panels a and c show the same time-step.

The spatial temperature distribution due to the combined influences of hydrogeological variation, seasonal temperature oscillations, and anthropogenic heat sources is depicted from a range of vantage points to highlight the extent of influence of these heat sources. Figure 5a shows the in-plane temperature distribution at a depth of $z = -5$ m from ground level for a single time-step of the simulation (after 20 years of simulation). The variation of temperature within the domain is apparent, with an evident temperature increase due to the presence of basements. Further, notable wakes of higher temperatures are seen in the northeast and northwest areas, driven mainly by groundwater flow, while the basements in the southern part of the domain exhibit a more distinct 'halo' of temperature increase compared to basements in the northern part, due to absence of significant groundwater flow at this depth, the consequence of a lower hydraulic conductivity in this region. This lower hydraulic conductivity results in zones of elevated temperatures closely equivalent to the basement footprints, as the primary heat transfer that takes place is conductive in nature.

Figure 5b shows temperature profiles at the location indicated by the blue dot in Figure 5a, over a series of one-month time-steps for the final year of the simulation, with each profile in the figure representing results at a different time-step. The range of temperatures produced by the seasonal temperature variation applied at the upper-most layer is apparent, as is a deviation of the average temperature from the mean ground temperature $T_{0,\mathrm{g}} = 12.9$ °C in the shallow layers of the model. This deviation at the shallow layers is a result caused predominantly by the presence of heated basements in the vicinity of the sampling point which acts to raise the mean temperature in the shallow layers. This temperature increase in the shallow subsurface is also apparent in Figure 5c, which depicts the temperature distribution within a slice through the model domain along the blue dashed line indicated in Figure 5a, again for the final time-step of the simulation. The influence of the presence of basements is again visible, with the ground temperatures in the western (left) side increased notably in the first 15 m below ground and, to a lesser extent, even as deep as 35 m. In contrast, on the eastern (right) side of the plot, where no basements are present in the vicinity of the slice, significant temperature increases are not seen any deeper than the first few metres below the surface. This stored heat in areas near heated basements may be potentially accessed using GHEs towards fulfilling heating demands of the area.

In determining temperatures of the shallow subsurface, and the possibly increased potential for geothermal energy due to anthropogenic influences, modelling choices can have significant impacts on results obtained from the numerical model. This section investigates in detail the effect that modelling choices have on model outputs. The influence of modelling choices is invariably governed by the chosen scale and resolution of model outputs. Hence, two scales are considered in the subsequent analyses: a 'point-based' (or 'local') and a 'domain-based' (or 'global') scale. The point-based scale focuses on smaller area effects used, for example, when analysing the temperature profile at a particular location due to an interest in that locality, particular area features, or when in-situ data is available which are typically measured within boreholes, *i.e.* point locations. The domain-based scale assesses the modelled area as a whole, looking at increased temperatures over (and heat fluxes into) the entire domain, which are useful for more general analyses, such as assessing the geothermal energy potential at city scale. Throughout the analyses, the effect of the three modelling simplifications, detailed in Section 2.3, is investigated to identify their suitability for both local and global modelling purposes. The outcomes of the analyses show that the two scales are affected in different ways by the modelling choices, with the point-based scale showing a greater sensitivity to simplifications.

3.1. Point-based model evaluation

In this section the impact of model simplifications on the ability of the numerical model to predict local temperature variation is evaluated. Model outputs are compared with temperature time-series data from 24 measurement locations throughout the domain [43], shown in Figure 6a with sensor depth indicated in the legend. Examples of the data measured are shown in Figures 6b and 6c. For each location, the data are fitted with an increasing/decreasing sine function for the temperature T (°C) as a function of time t in days, $T(t) = T_{\text{amp}} \sin\left(\frac{2\pi}{365}t + \phi_T\right) + T_{\text{inc}}\left(t - t_{\text{start}}\right)$, and the fitting parameters found, *i.e.* the mean temperature T_{mean} (°C), the amplitude of temperature fluctuation T_{amp} (°C), the phase ϕ_T (rad), and the annual temperature increase T_{inc} (°C). The frequency in all cases is set to that of the seasonal temperature oscillation at the surface. The fitted sine waves are shown alongside the measured data in Figures 6b and 6c, with fitting parameters T_{mean} and T_{amp} indicated. This fitting is also performed for modelled temperature data at the same locations for each of the 8 different combinations of modelling choices outlined in Section 2.3, giving rise to the same four wave parameters for each model combination (see figures). Of the fitted parameters, the ones of most interest to the investigation of the subsurface are the mean and the amplitude of the temperature oscillation. These two parameters are more indicative for the thermal conditions over time of a location than single time temperature measurements.

As a measure of the ability of a given model combination to accurately predict the measured temperature, the absolute error between the measured and the modelled fitting parameters at a location is determined. For example, the model shown in Figure 6c exhibits an absolute error in the mean temperature of $e_{T_{\text{mean}}} = |T_{\text{mean, model}} - T_{\text{mean, data}}| = 1.65$ °C. To measure the response of model output to a single type of simplification (elevation, hydraulic head distribution, and basement geometry), changes in absolute error values for the models are combined into a single value by calculating the change in error between models with only one simplification applied, and averaging across the different model combinations. For example, the response of the absolute error in mean temperature to simplification of the elevation implementation $\Delta e_{\text{E},T_{\text{mean}}}$ (°C) is calculated by averaging the differences in error between each pair of models, one with realistic and one with simplified elevations, with the same hydraulic head and basement geometry implementations *i.e.*

$$\Delta e_{\text{E},T_{\text{mean}}} = \frac{\sum\limits_{i,j}^{\{\text{R,S}\}} \left(e_{T_{\text{mean},\text{E}_\text{S}\text{H}_i\text{B}_j}} - e_{T_{\text{mean},\text{E}_\text{R}\text{H}_i\text{B}_j}}\right)}{\sum \text{Model combinations}}. \tag{15}$$

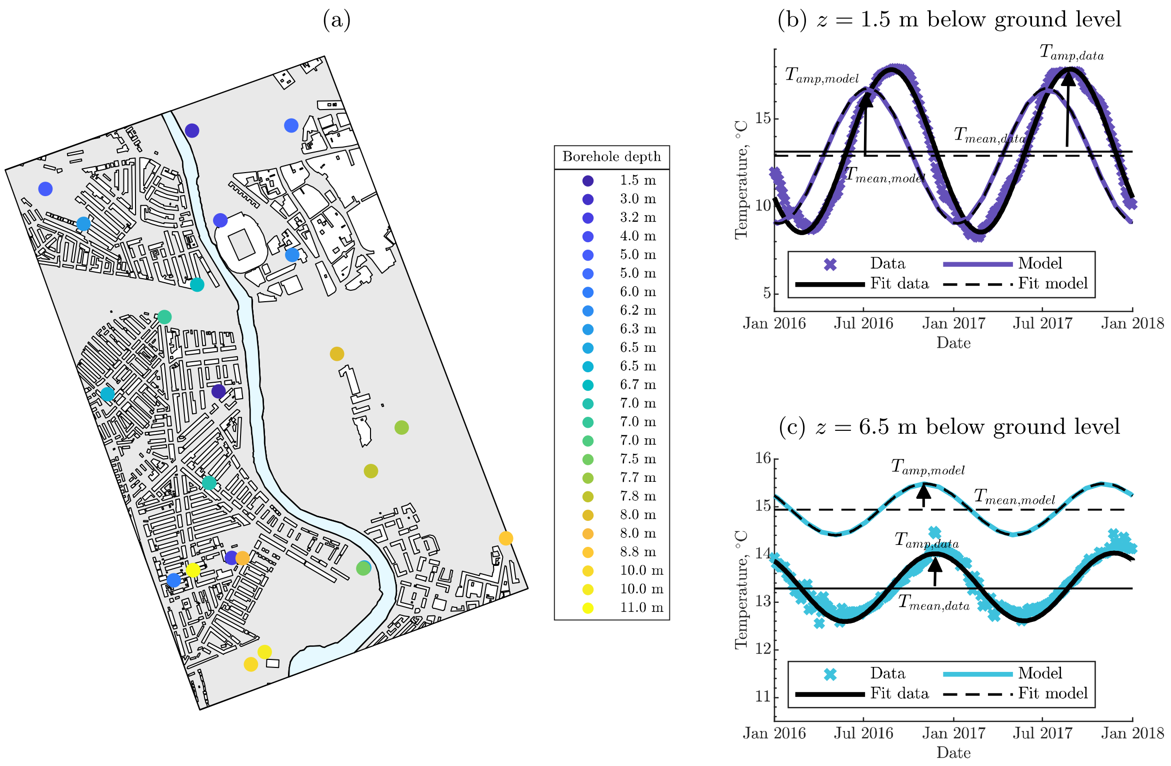

Figure 6: Measurement locations in domain with colour denoting depth of sensor (left panel) and examples of data fitting (right two panels).

This is performed for each simplification and error responses along each dimension of simplification space are determined.

Across the 24 measurement locations, simplifications affect the model results differently due to the variations in surrounding hydrogeological characteristics, proximity to heat sources, depth of measurement point, etc. To identify common responses of model outputs at the measurement points due to simplifications, the 24 points are clustered hierarchically according to the error response in each of the three simplification dimensions. This results in a set of dendrograms for each wave parameter of interest, *i.e.* mean temperature and temperature amplitude, shown in Figures 7a and 7e. The leaves of the dendrograms are labelled with the depths of the measurement location associated with each leaf. The corresponding spatial distribution of clusters is shown in Figures 7b-7d for the response of mean temperature, and in Figures 7f-7h for temperature amplitude, along with the associated cluster centroids in the error change space. The centroids $(\Delta e_{\mathrm{E}}, \Delta e_{\mathrm{H}}, \Delta e_{\mathrm{B}})$ give the euclidean centre of the clusters in the error response space due to

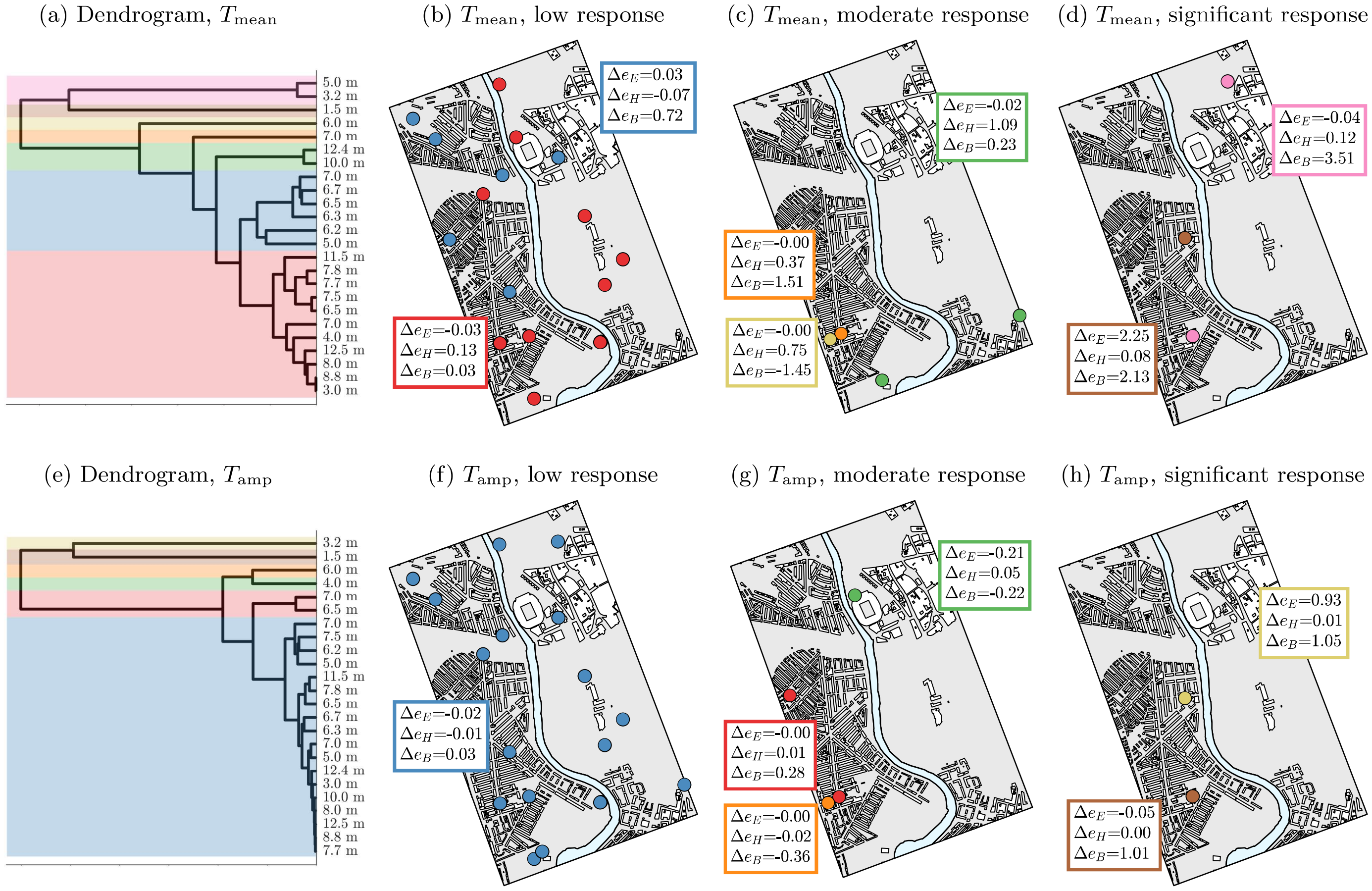

Figure 7: Cluster structure of 24 measurement points in the domain for mean temperature (panel a) and temperature oscillation amplitude (panel e) and spatial distribution of clusters (panels b, c, d, and f, g, h respectively). © Crown copyright and database rights 2021 Ordnance Survey [100021290 EUL]. Use of this data is subject to terms and conditions.

simplification of the elevation resolution of the numerical model (E), simplification in the hydraulic head distribution (H), and simplification in the basement representation (B).

The majority of the 24 points exhibit a low error response to simplification in mean temperature of less than $|\Delta e_{T_{\text{mean}}}| < 1$ °C in any one of the simplification error dimensions, as seen in Figure 7b where the two clusters presented have centroids at $(-0.03, 0.13, 0.03)$ and $(0.03, -0.07, 0.72)$. These points span a range of depths and are located in various different geological materials, indicating that the impact of model simplifications are not significant at locations under the majority of conditions found in the domain. The results also show that the error is not consistently increasing or decreasing with depth alone. Points with a moderate response in mean temperature, *i.e.* 1 °C $\leq |\Delta e_{T_{\text{mean}}}| < 2$ °C, are presented in Figure 7c. The locations exhibit a response to simplification in basement distribution on the one hand (*i.e.* the orange and yellow locations with centroids $(0.00, 0.37, 1.51)$ and $(0.00, 0.75, -1.45)$, respectively), and on the other a response in hydraulic distribution (green locations with centroid $(-0.02, 1.09, 0.23)$). Significantly impacted locations, with $|\Delta e_{T_{\text{mean}}}| > 2$ °C, shown in Figure 7d all exhibit a high sensitivity to simplifications to heat source geometry. As with the locations moderately impacted by basement distribution, these points are located in the shallower layers and closer to basements. However, the considerably impacted locations are outside of areas of significant groundwater flow (aquifer) such that the dominant heat transfer is conductive (further indicated by the low sensitivity to hydraulic distribution), indicating that, in locations that are proximate to heat sources where conduction dominates, heat source geometry has a considerable impact on accurate temperature predictions. In contrast with the shallower points exhibiting a low response to basement simplifications, the pink points (centroid $(-0.04, 0.12, 3.51)$) are not uniformly surrounded by basements and thus not within a homogeneous ground temperature increase. The brown outlier point (centroid $(2.25, 0.08, 2.13)$) is the shallowest in the whole domain at 1.5 mbgl and closest point to a heated basement (NB: the basement of the stadium is unheated) outside of the aquifer, confirming the importance of conduction when considering heat source representation.

Regarding the response of temperature amplitude, it is again apparent that a majority of the locations are insensitive to simplifications, as seen in Figure 7f. Save one, these locations are all within the aquifer and hence either fairly far from heat sources or within convection dominated regions. However, of the points that do show a appreciable response, the response is always to basements geometry. This is most likely due to the shielding effect that a heated basement has to the temperature fluctuation from the surface. For all locations considered, none showed a meaningful response to hydraulic distribution implemented by the model. This indicates that the direction of groundwater flow is not as important when modelling for temperature fluctuation amplitude, provided groundwater flow is captured.

It may be noted that the majority of the locations exhibit some response, for both mean temperature and amplitude, to changes in basement simplification, albeit small in some cases. This indicates that accurate representation of heat sources is one of the more important aspects in the numerical modelling to implement correctly, while also being one of the more difficult due to the considerable uncertainty associated. The error response to changes in hydraulic distribution is low for most locations shown in the domain. This is likely a result of the moderate groundwater flow in the aquifer, generating only modest temperature wakes downstream of basements. For very high magnitudes of groundwater flow velocities, it is to be expected that the impact of groundwater flow is also low due to the dispersion of the higher temperature groundwater through the domain. It is likely that for moderately fast groundwater flow velocities the impact of simplification of hydraulic distribution increases and peaks before decreasing again for very high flow speeds. Finally, it is notable that most of the error responses shown in Figure 7 are positive, which means that simplifications produce outputs with a greater deviation from measured temperatures than realistic implementation, in some cases significantly so. The only reduction in error occurs for very few moderate and low responses. Overall, the results indicate that in absence of significant groundwater flow, simplifications must be considered more carefully, in particular regarding correct representation of heat sources.

3.2. Domain-based model evaluation

The effect of the anthropogenic influence on the entirity of the modelled domain is investigated in this section, in addition to how adoption of modelling simplifications can affect model outputs. Given that the focus of this research is on thermal effects of anthropogenic infrastructure in the shallow subsurface, and therefore the temperature of the ground, a natural initial metric to consider for this analysis is the overall temperature within the modelled domain. Therefore, the

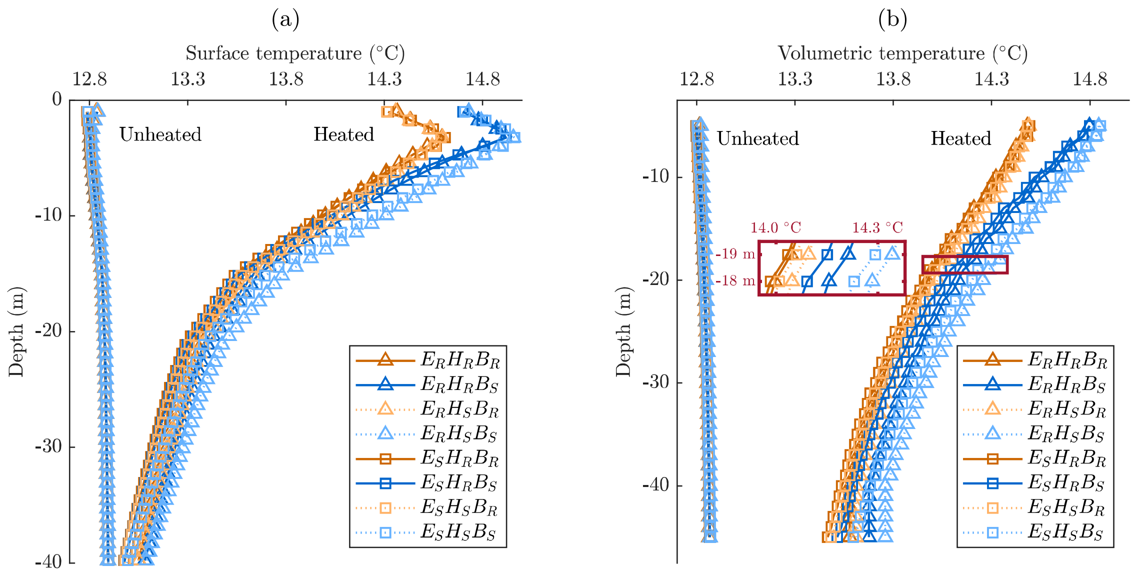

Figure 8: Global analysis: Average surface (panel a) and volumetric (b) temperature with depth for each model, averaged over the last year of simulation. (Model name abbreviations as defined in Section 2.3.)

average temperature of the ground, in terms of a surface average (*i.e.* over the x and y dimensions for each layer) and a volume average (*i.e.* over the (x, y, z) dimensions, from the surface down to z for each value) are calculated and discussed. These constitute an aggregate measure on the extent of propagation of temperature anomalies into the ground as well as an indication of the thermal state of the domain subsurface. Figure 8 shows these metrics in panels (a) and (b) respectively, averaged over the final year of the simulations. In both figures, results for each model are shown with both unheated (left group of lines) and heated basements (right group of lines). Unsurprisingly, in the absence of heated basements, temperature volume averages show near no differences irrespective of the simplifications adopted and are very close to the annual mean temperature of 12.9 °C. When heated basements are implemented, the temperatures are greatest near the surface, where basements are located and where the surface temperature is applied to the ground, and converge towards the annual mean with increasing depth. Temperature surface averages for models incorporating heated basements spike around 4 m, just below the lower edge of the 3 m deep basements and at approximately the depth at which groundwater flow is introduced.

The results indicate that the presence of heated basements can increase the temperature of the ground for the first few tens of meters below the surface. For example, within the first 30 m below ground level, the volumetric temperature average increase caused by the heated basements varies between about 0.86 and 1.11 °C, depending on the modelling choices. Nearer the surface, basement geometry simplification proves to be most impactful of the simplifications investigated, with differences in temperatures of near 0.4 °C as the lines of same colours (*i.e.* with the same basement geometry) cluster together in the figures. At 4 m below the surface, where groundwater is introduced, the effect of the hydraulic simplification becomes apparent, as the solid and dashed (or darker/lighter) lines of the same colour, indicating realistic and simplified implementations of hydraulic head distribution in the model, respectively, diverge from one another with increased depth. The inset in 8b shows a close-up of the impact of each simplification. As can be seen, simplifying the basement and hydraulics both results in higher temperatures (differences of up to 0.25 °C and 0.15 °C respectively at a depth of 19 m), while simplifying the elevation results in slightly lower temperatures. However, the temperature difference from simplifying the elevation is notably smaller than the other two, while the basement simplification is shown to cause the largest discrepancies. The results further suggest that the impact of elevation modelling depends on the basement modelling choice, as the two dark orange lines and the two light orange lines are closer together compared to the blue ones, indicating that if the basements are realistically modelled, a simplification in elevation (and thus reduction in computational time) is more justifiable. From a point of view of the overall increase in volumetric ground temperature, in this study the impact of the modelling simplifications is within reason, resulting in a maximum change of no more than 0.5 °C. However, over longer simulation periods (and thus greater heat accumulation) the difference between these results is likely to become more significant.

A further metric to consider at the domain scale is the heat flux into the ground due to the presence of basements. This is shown in Figure 9 as the average heat flux over the entire domain for four values of depth from the surface (z). As is to be expected, heat flux values are higher in the shallower levels, closer to the heat sources, and reduce in magnitude in the deepest layers. Comparing the heat fluxes across the models at the two shallowest layers, 6 m and 11 m below the surface (two lightest colour bars in figure), it is interesting to observe similar magnitudes of average heat flux into the ground. The presence of groundwater flow within the aquifer between about 5 and 10 m below the surface likely affects the downwards heat flux, as some of the heat from the basements is moved via convection downstream. Moreover, nearer the surface both upwards and downwards heat fluxes exist, due to the surface and radial heat from the basements, which further affects the domain average downward heat flux. Through comparison between models implementing realistic and simplified basement representation the choice of basement geometry

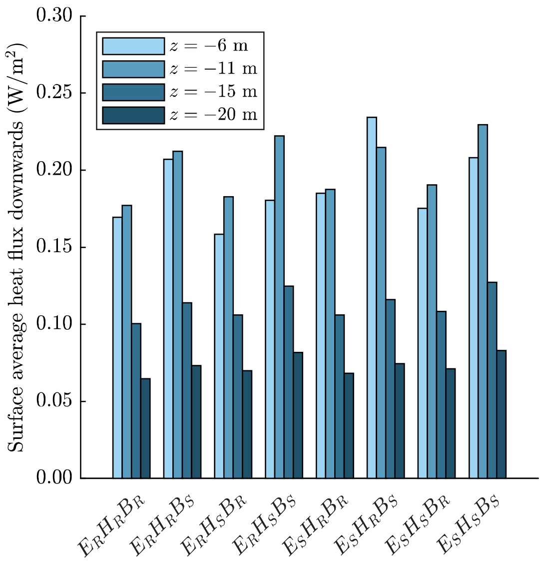

Figure 9: Average heat fluxes downwards, over a horizontal plane at four different depths, z.

is seen to be the most impactful, suggesting that the exact shape and location of the basements, as well as the distance between them, can affect the heat flux into the ground. The likely cause of this is that the simplified basement distribution used in this study is more homogeneous and covers a wider area of ground, despite the total heated basement area remaining the same. While this difference is relatively small and reduces with depth below 11 m, when considering the size of the area modelled (3.5 km^2) the cumulative impact of the difference can be significant, depending on the context of the investigation.

An important aspect of exploring anthropogenic influence on subsurface temperatures is the chance of an increase in shallow geothermal potential and the possibility of utilising it more efficiently. Shallow geothermal energy and ground-source heat pumps use the ground as a heat source or sink to provide clean heating and cooling to buildings and are becoming increasingly popular as the world moves towards employing more renewable sources of energy. A common type of shallow geothermal energy systems consists of vertical borehole ground heat exchangers (GHEs) which transfer heat to/from the ground, connected to a ground-source heat pump to transfer the heat from/to buildings via ventilation systems. It is of interest to assess how increased average ground temperatures due to the presence of heated basements can affect the design and effectiveness of borehole GHEs. To calculate the geothermal potential of the modelled area, a

Table 2: Parameters used in the geothermal potential calculations using Equation 16, for a single borehole of about 30 m, based on typical values [62–64]

Design parameters [units]	Description	Values
q_h [W]	Peak hourly ground load	954
q_m [W]	Monthly averaged ground load	477
q_y [W]	Yearly averaged ground load	119
R_b [m·K/W]	Effective thermal resistance of the borehole (standard U-loop)	0.103
R_{6h} [m·K/W]	Effective thermal resistance of the ground to 6 hours of ground load	0.10
R_m [m·K/W]	Effective thermal resistance of the ground to 1 month of ground load	0.15
R_y [m·K/W]	Effective thermal resistance of the ground to 10 years of ground load	0.18
T_m [°C]	Mean fluid temperature of borehole	3
T_g [°C]	Ground temperature	varies*
T_p [°C]	Temperature penalty for borehole field	-0.25

*Values based on Figure 8b at depth of 30 m widely used analytical solution introduced by [62] and [63] is adopted, expressed as

$$L = \frac{q_h R_b + q_y R_{10y} + q_m R_{1m} + q_h R_{6h}}{T_m - (T_g + T_p)}, \tag{16}$$

for which the parameters are defined in Table 2, based on typical values for a standard single-loop borehole configuration and the conditions of the site. The load parameters are based on values for heating, which is the dominant mode in the region considered.

Using this process and the data outlined above, two metrics are computed assessing geothermal potential: the savings in drilling costs (assuming a cost of £70/m) as and the additional geothermal energy that can be provided by GHEs. The latter is calculated by assuming a constant borehole length of 30 m and by varying, or rather scaling, the thermal load that can be provided. For the purpose of this analysis a borehole length of 30 m is assumed and multiple boreholes are grouped together within a field to provide the required energy for a given system. To satisfy the space heating demand (assuming constant temperature levels) for a typical semi-detached modern house in Cardiff [65], about 10 such boreholes would be required. The analysis compares the benefit of installing these systems within an anthropogenically influenced domain by comparing the borehole length/geothermal potential results from two simulations for each modelling choice combination, one with heated and one with unheated basements.

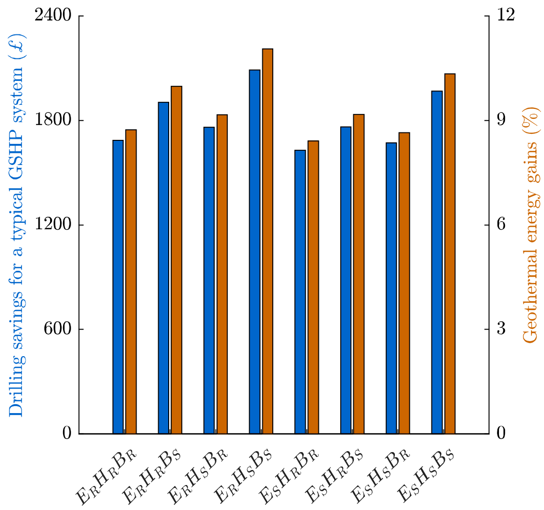

Figure 10: Comparison of geothermal energy potential due to anthropogenic heat sources (compared to an absence of heat sources), for the three modelling simplifications. Results are shown in terms of the drilling cost savings for a typical ground-source heat pump system (left axis) and the additional geothermal energy that can be gained due to the anthropogenic influence (right axis).

The results of the geothermal potential investigation are presented in Figure 10, with the left y-axis showing cost savings and the right showing gains in geothermal energy. Overall, the presence of heated basements is beneficial to the utilisation of GSHP systems, with lower installation costs and greater thermal energy provision potential. This is expected given the heating dominant demand, which requires drawing heat from the ground, facilitated by higher ground temperatures. The benefits consist of savings in drilling costs between about £1630 and £2090 for a GSHP system in a typical semi-detached modern house and an increase in the geothermal energy potential of between 8.5% and 11%. These values are consistent, in terms of the percentage of borehole length reduction, with [22], albeit at the lower range of the reported findings. It is worth noting here that calculating the energy potential at a domain level may lead to an underestimate of the benefits that some local regions with higher ground temperatures may experience. A strategic approach could be employed to identify these particular areas and utilise their geothermal potential more efficiently, using more complex modelling methodologies to quantify this potential. These additional considerations will be investigated in detail in future work. Regarding the modelling simplifications, it can be seen that, despite values being relatively close, some discrepancies exist. While the choice of elevation modelling has a very minor impact, the basement and hydraulic simplifications do affect the estimations for savings and energy gains, with higher benefits predicted when simplified modelling is adopted. Simplifying both of these modelling choices results in the highest estimation for geothermal benefits. In the context of assessing the geothermal potential at city-scale, a partly simplified numerical model can be confidently adopted. However, if multiple aspects of the model are to be simplified, including both hydraulics and basement geometry, this should be done acknowledging that results could overestimate the geothermal potential.

3.3. Computational time comparison

A crucial consideration in numerical modelling and how accurately a scenario can be modelled is the computational time and power required by a model. In this analysis high-performance computing has been utilised with 32 cores of 2.4 GHz processing power each. The computational time required for each model is shown in Table 3, combined with the number of mesh elements per layer as well as the total number of layers (noting that for E_R models the surface layers have only partial areas activated as part of modelling elevation). As expected, a lower number of mesh elements (and thus fewer degrees of freedom) and layers result in shorter computational

Table 3: Computational time required to run the numerical models on a high performance computing (32 cores - 2.4 GHz)

Model name	Mesh element no. [-]	No. of layers [-]	Comp. time with heated basements [HH:MM]	Comp. time with unheated basements [HH:MM]
$E_R H_R B_R$	43827	33	4:54	4:35
$E_R H_R B_S$	56193	33	5:42	5:45
$E_R H_S B_R$	43827	33	4:34	4:35
$E_R H_S B_S$	56193	33	5:34	5:49
$E_S H_R B_R$	38451	23	3:44	3:40
$E_S H_R B_S$	39007	23	4:00	3:50
$E_S H_S B_R$	38451	23	3:30	3:35
$E_S H_S B_S$	39007	23	3:38	3:50

times, following a close-to-linear relationship. Due to the nature of computational analysis and the algorithms used, the exact time required varies slightly between identical simulations. A significant change in computational time is observed for changes in the elevation modelling choice, since realistic elevation modelling includes a greater number of layers and thus more degrees of freedom. A notable difference is also observed with regards to basement geometry simplification. In this scenario, the simplified basement geometry results in more mesh elements compared to the realistic (using consistent meshing techniques), and therefore longer computational times which, albeit unusual, demonstrates that simplified conditions do not guarantee computational savings. The data demonstrates the potential savings in time that can be achieved by given modelling choices and simplifications, in situations where these are acceptable, depending on the purpose and accuracy requirements of the modelling work.

4. Conclusion

A better understanding of how the subsurface can be modelled allows for improved quantification of the anthropogenic influence on it, as well as for the identification of potential opportunities, such as more efficient use of shallow geothermal energy. However, measured data of the subsurface is often prohibitively difficult to obtain, creating uncertainties on the exact hydrogeological conditions. Moreover, high computational requirements associated with city-scale modelling are often restrictive. Therefore, when utilising numerical modelling to model the subsurface at city-scale, it is common practice to adopt a number of simplifications to compensate for the lack of knowledge about an area and reduce computational costs. This work contributes towards a better understanding of subsurface modelling by investigating the implementation of three common simplifications: the resolution in modelling surface elevation, the geometry of basements, and the hydraulic head distribution. The impact of each modelling simplification is considered in terms of accuracy at a point (local) scale and a domain (global) scale, depending on the purpose behind the study, as well as the associated computational costs. Modelling at these two scales provides insights for different purposes. The local scale allows comparison with and validation against measured data, where accurate prediction of temperatures at specific locations becomes important, as well as investigating localised conditions and groundwater impacts, for example for the purpose of designing a GSHP system for a household. At the larger scale, modelling can inform city planning by exploring large scale impacts due to infrastructure development, for example defining the geothermal potential at a city scale, as well as how this may contribute to the urban underground heat island effect. The central area of Cardiff, UK, has been used as a case study for this work, implementing data available for the area as well as measured temperatures from in-situ monitoring and including the modelling of the river Taff, flowing through the centre of the modelled domain.

Numerical modelling of the subsurface at city-scale produces a large volume of data, allowing for analyses from different angles and at different scales. A point-based evaluation is used to explore the effect of simplifications on temperatures at specific (x, y, z) locations within the domain. In this work, 24 points for which measured data are available are considered, and numerical simulations with both realistic and simplified modelling choices are performed. A sinusoidal wave is fitted to the resulting temperatures time-series, and wave parameters are compared to those determined from measured data at these points. The points are subsequently clustered according to the response of the discrepancies between modelled and measured results to modelling simplifications, to identify commonalities between the behaviours across different conditions. Overall, for the majority of the points considered, the realistic and simplified models produce similar outputs, in particular for simplifications in the model elevation implementation. The results suggest that the presence of groundwater flow mitigates the use of simplifications for the other features, likely because a significant flow distributes heat over a greater area and reduces localised effects. Points in the area outside the aquifer show more sensitivity to the other simplifications. In particular, points in the shallower layers of the subsurface, which are outside the aquifer and closest to basements, exhibit a sensitivity to the representation of basement geometry, with differences in the mean ground temperature of up to 3.5 °C. Regarding the amplitude of the temperature wave, it is shown that the modelling of the basement geometry can be an important parameter for specific points, likely due to how the geometry as well as the shallower ground temperature affect surface temperature fluctuations reaching deeper layers of the subsurface. The results indicate that, when modelling a large subsurface area with the purpose of determining the temperature at specific points, an understanding of heat source geometries and hydrogeological conditions around those points is crucial. Importantly, if no groundwater flow is present around the points and conductive heat transfer processes dominate, modelling simplifications could result in significant discrepancies.

At the domain-scale, referring to the modelled domain holistically instead of at individual point locations, this work investigates both the effect of the anthropogenic sources (heated basements) on the subsurface as well as at what degree the modelling simplifications affect these results. For each of the eight cases (adopting different combinations of simplifications) a simulation is run with heated basements and with unheated basements (for a total of 16 models). The average ground temperature is computed for each simulation and plotted over the depth, in terms of the average surface temperature of each layer and the average volumetric temperature beginning from the surface. The results show that, for averaged temperatures, simplifying the basement geometry and the hydraulic head distributions can overestimate the computed temperatures by up to 0.4 °C and 0.2 °C, respectively, the former being more impactful at shallow levels and the latter increasing in importance at deeper levels, where groundwater flow is introduced, while simplifying the elevation has little impact. Using a simplified basement geometry distribution is seen to have the greatest effect of the three simplifications, which is consistent with the findings of the local-scale analysis. The surface averaged heat flux into the ground at different depths is found to be approximately 0.06 W/m^2 at 20 m depth across all models, but exhibits sensitivity to the basement geometry simplification. As part of the analysis, the geothermal potential of the domain is calculated, implementing a widely used analytic solution to compute the length of a typical vertical borehole for the different values of average ground temperature of the different models. The results are shown in terms of the drilling cost savings as well as the geothermal energy gains resulting from the increase in ground temperature and assuming heating dominant conditions. It is shown that the anthropogenic heat sources can reduce drilling costs for a typical house GSHP system by about £1700 and increase the geothermal energy potential by about 9%. The simplifications used in the modelling tend to overestimate these gains/savings, with ranges in savings between £1630 and £2090 and in geothermal potential between 8.5% and 11%, noting that simplifying both the hydraulic head and basement distributions leads to the furthest values from the realistic models. This suggests that, for the purpose of estimating the geothermal potential at city scale, given the magnitude of the values, the adoption of some modelling simplifications can be appropriate, however simplifying both the hydraulic conditions and the basement should be either avoided if possible or, if adopted, acknowledging the potential for overestimation.

This work has presented the potential anthropogenic impact on the subsurface, at different scales, as well as investigated common simplifications adopted in its numerical modelling. However, it is worth noting here that even in cases where data and information about the local conditions exist, as in this work, it is still difficult to gain sufficient knowledge for all required modelling parameters. The heterogeneity of real materials and conditions can create difficulties for city-scale modelling. For example, the presented analysis demonstrates how different locations can be affected differently from anthropogenic influence and therefore inferring city scale parameters from single or limited point measurements can be misleading. Therefore, future work aim to undertake calibration of important modelling parameters for this case study, using the relatively large set of measurement points to identify common patterns and gain insights on how to best model uncertainty in city-scale modelling.

Acknowledgements

This work was supported by CMMI-EPSRC: Modeling and Monitoring of Urban Underground Climate Change (EP/T019425/1), by the Centre for Smart Infrastructure & Construction (EP/N021614/1) and the Centre for Digital Build Britain at University of Cambridge, as well as AI for Science and Government (ASG), UKRI's Strategic Priorities Fund awarded to the Alan Turing Institute, UK (EP/T001569/1). The authors are grateful to Ricky Terrington (BGS) and Dave Boon (BGS) for their valuable input to the data acquisition for this work and to Cardiff Harbour Authority for provision of supporting data and access to boreholes. Gareth Farr and Johanna Scheidegger publish with the permission of the executive director, BGS, UKRI.

References

[1] D. Krcmar, R. Flakova, I. Ondrejkova, K. Hodasova, D. Rusnakova, Z. Zenisova, M. Zatlakovic, Assessing the Impact of a Heated Basement on Groundwater Temperatures in Bratislava, Slovakia, Groundwater 58 (2020) 406–412.

[2] P. Bayer, G. Attard, P. Blum, K. Menberg, The geothermal potential of cities, Renewable and Sustainable Energy Reviews 106 (2019) 17–30.

[3] T. Arola, K. Korkka-Niemi, L'effet des îles de chaleur urbaine sur le potentiel géothermique: exemples d'aquifères quaternaires en Finlande, Hydrogeology Journal 22 (2014) 1953–1967.

[4] E. Romero, A. Gens, A. Lloret, Temperature effects on the hydraulic behaviour of an unsaturated clay, Geotechnical and Geological Engineering 19 (2001) 311–332.

[5] A. Colmenar-Santos, M. Folch-Calvo, E. Rosales-Asensio, D. Borge-Diez, The geothermal potential in Spain, Renewable and Sustainable Energy Reviews 56 (2016) 865–886.

[6] K. Menberg, P. Bayer, K. Zosseder, S. Rumohr, P. Blum, Subsurface urban heat islands in German cities, Science of the Total Environment 442 (2013) 123–133.

[7] M. Taniguchi, J. Shimada, Y. Fukuda, M. Yamano, S. i. Onodera, S. Kaneko, A. Yoshikoshi, Anthropogenic effects on the subsurface thermal and groundwater environments in Osaka, Japan and Bangkok, Thailand, Science of the Total Environment 407 (2009) 3153–3164.

[8] S. A. Benz, P. Bayer, K. Menberg, S. Jung, P. Blum, Spatial resolution of anthropogenic heat fluxes into urban aquifers, Science of the Total Environment 524-525 (2015) 427–439.

[9] G. Attard, Y. Rossier, T. Winiarski, L. Eisenlohr, Deterministic modeling of the impact of underground structures on urban groundwater temperature, Science of the Total Environment 572 (2016) 986–994.

[10] B. Kløve, P. Ala-Aho, G. Bertrand, J. J. Gurdak, H. Kupfersberger, J. Kværner, T. Muotka, H. Mykrä, E. Preda, P. Rossi, C. B. Uvo, E. Velasco, M. Pulido-Velazquez, Climate change impacts on groundwater and dependent ecosystems, Journal of Hydrology 518 (2014) 250–266.

[11] F. Tinti, A. Barbaresi, S. Benni, D. Torreggiani, R. Bruno, P. Tassinari, Experimental analysis of shallow underground temperature for the assessment of energy efficiency potential of underground wine cellars, Energy and Buildings 80 (2014) 451–460.

[12] T. Vienken, F. Händel, J. Epting, P. Dietrich, R. Liedl, P. Huggenberger, Energiewende braucht Wärmewende – Chancen und Limitierungen der intensiven thermischen Nutzung des oberflächennahen Untergrundes in urbanen Gebieten vor dem Hintergrund der aktuellen Energiedebatte in Deutschland, Grundwasser 21 (2016) 69–73.

[13] A. Bidarmaghz, G. Narsilio, Heat exchange mechanisms in energy tunnel systems, Geomechanics for Energy and the Environment 16 (2018) 83–95.

[14] N. Makasis, Further understanding ground-source heat pump system design using finite element methods and machine learning techniques, Ph.D. thesis, PhD Thesis, The University of Melbourne, 2019.

[15] N. Makasis, G. A. Narsilio, Investigating the thermal performance of energy soldier pile walls, Geomechanics for Energy and the Environment (2020) under review.

[16] A. Gryc, K. Was, J. Radon, Experimental research on thermal conditions in intermittently heated basement, Infrastructure and ecology of rural areas 12 (2011) 135 – 145.

[17] G. Ferguson, A. D. Woodbury, Subsurface heat flow in an urban environment, Journal of Geophysical Research: Solid Earth 109 (2004) 1–9.

[18] M. Barla, A. Di Donna, M. Baralis, City-scale analysis of subsoil thermal conditions due to geothermal exploitation, Environmental Geotechnics 7 (2020) 306–316.

[19] K. Menberg, P. Blum, A. Schaffitel, P. Bayer, Long-term evolution of anthropogenic heat fluxes into a subsurface urban heat island, Environmental Science and Technology 47 (2013) 9747–9755.

[20] A. Bidarmaghz, R. Choudhary, K. Soga, H. Kessler, R. L. Terrington, S. Thorpe, Influence of geology and hydrogeology on heat rejection from residential basements in urban areas, Tunnelling and Underground Space Technology 92 (2019) 103068.

[21] F. Ampofo, G. Maidment, J. Missenden, Underground railway environment in the uk part 2: Investigation of heat load, Applied Thermal Engineering 24 (2004) 633 – 645.

[22] J. A. Rivera, P. Blum, P. Bayer, Increased ground temperatures in urban areas : Estimation of the technical geothermal potential, Renewable Energy 103 (2017) 388–400.

[23] Y. Zhang, K. Soga, R. Choudhary, Shallow geothermal energy application with GSHPs at city scale: study on the City of Westminster, Géotechnique Letters 4 (2014) 125–131.

[24] M. H. Mueller, P. Huggenberger, J. Epting, Combining monitoring and modelling tools as a basis for city-scale concepts for a sustainable thermal management of urban groundwater resources, Science of the Total Environment 627 (2018) 1121–1136.

[25] T. Vienken, M. Kreck, P. Dietrich, Monitoring the impact of intensive shallow geothermal energy use on groundwater temperatures in a residential neighborhood, Geothermal Energy 7 (2019).

[26] B. Meng, T. Vienken, O. Kolditz, H. Shao, Evaluating the thermal impacts and sustainability of intensive shallow geothermal utilization on a neighborhood scale: Lessons learned from a case study, Energy Conversion and Management 199 (2019) 111913.

[27] A. García-Gil, M. Mejías Moreno, E. Garrido Schneider, M. A. Marazuela, C. Abesser, J. Mateo Lázaro, J. A. Sánchez Navarro, Nested shallow geothermal systems, Sustainability 12 (2020).

[28] C. Tissen, K. Menberg, S. A. Benz, P. Bayer, C. Steiner, G. Götzl, P. Blum, Identifying key locations for shallow geothermal use in vienna, Renewable Energy 167 (2021) 1–19.

[29] A. Ramos-Escudero, M. S. García-Cascales, J. M. Cuevas, B. Sanner, J. F. Urchueguía, Spatial analysis of indicators affecting the exploitation of shallow geothermal energy at european scale, Renewable Energy 167 (2021) 266–281.

[30] J. Epting, M. Baralis, R. Künze, M. H. Mueller, A. Insana, M. Barla, P. Huggenberger, Geothermal potential of tunnel infrastructures – development of tools at the city-scale of Basel, Switzerland, Geothermics 83 (2020) 101734.

[31] J. Epting, A. García-Gil, P. Huggenberger, E. Vázquez-Suñe, M. H. Mueller, Development of concepts for the management of thermal resources in urban areas – Assessment of transferability from the Basel (Switzerland) and Zaragoza (Spain) case studies, Journal of Hydrology 548 (2017) 697–715.

[32] J. Epting, S. Scheidler, A. Affolter, P. Borer, M. H. Mueller, L. Egli, A. García-Gil, P. Huggenberger, The thermal impact of subsurface building structures on urban groundwater resources – A paradigmatic example, Science of the Total Environment 596-597 (2017) 87–96.

[33] S. A. Benz, P. Bayer, F. M. Goettsche, F. S. Olesen, P. Blum, Linking Surface Urban Heat Islands with Groundwater Temperatures, Environmental Science and Technology 50 (2016) 70–78.

[34] K. Zhu, P. Bayer, P. Grathwohl, P. Blum, Groundwater temperature evolution in the subsurface urban heat island of Cologne , Germany, Hydrological Processes 29 (2015) 965–978.

[35] J. Epting, P. Huggenberger, Unraveling the heat island effect observed in urban groundwater bodies - Definition of a potential natural state, Journal of Hydrology 501 (2013) 193–204.

[36] J. Ondreka, M. I. Rüsgen, I. Stober, K. Czurda, GIS-supported mapping of shallow geothermal potential of representative areas in south-western Germany-Possibilities and limitations, Renewable Energy 32 (2007) 2186–2200.

[37] W. Zhan, W. Ju, S. Hai, G. Ferguson, J. Quan, C. Tang, Z. Guo, F. Kong, Satellite-derived subsurface urban heat island, Environmental Science and Technology 48 (2014) 12134–12140.

[38] G. Wang, G. Liu, Z. Zhao, Y. Liu, H. Pu, A robust numerical method for modeling multiple wells in city-scale geothermal field based on simplified one-dimensional well model, Renewable Energy 139 (2019) 873–894.

[39] J. Epting, F. Böttcher, M. H. Mueller, A. García-Gil, K. Zosseder, P. Huggenberger, City-scale solutions for the energy use of shallow urban subsurface resources – Bridging the gap between theoretical and technical potentials, Renewable Energy 147 (2020) 751–763.

[40] M. J. Kreitmair, N. Makasis, A. Bidarmaghz, R. L. Terrington, G. J. Farr, J. M. Scheidegger, R. Choudhary, Effect of anthropogenic heat sources in the shallow subsurface at city-scale, E3S Web of Conferences 205 (2020).

[41] A. M. Patton, G. J. Farr, D. P. Boon, D. R. James, B. Williams, L. James, R. Kendall, S. Thorpe, G. Harcombe, D. I. Schofield, A. Holden, D. White, Establishing an urban

geo-observatory to support sustainable development of shallow subsurface heat recovery and storage, Quarterly Journal of Engineering Geology and Hydrogeology 53 (2020) 49–61.

[42] G. J. Farr, A. M. Patton, D. P. Boon, D. R. James, B. Williams, D. I. Schofield, Mapping shallow urban groundwater temperatures, a case study from Cardiff, UK, Quarterly Journal of Engineering Geology and Hydrogeology 50 (2017) 187–198.

[43] G. J. Farr, A. Patton, D. P. Boon, D. R. James, L. Coppell, L. James, Cardiff urban geo-observatory, groundwater temperature data 2014-2018, 2019.

[44] R. S. Kendall, L. R. Williams, A. M. Patton, S. Thorpe, Metadata report for the cardiff superficial deposits 3d geological model, 2020. This item has been internally reviewed, but not externally peer-reviewed.

[45] A. Bidarmaghz, R. Choudhary, K. Soga, R. L. Terrington, H. Kessler, S. Thorpe, Large-scale urban underground hydro-thermal modelling – A case study of the Royal Borough of Kensington and Chelsea, London, Science of The Total Environment 700 (2020).

[46] Google, Map of UK from Google Maps, `https://www.google.com/maps/`, 2020. Last accessed 22 December 2020.

[47] G. Dalla Santa, A. Galgaro, R. Sassi, M. Cultrera, P. Scotton, J. Mueller, D. Bertermann, D. Mendrinos, R. Pasquali, R. Perego, S. Pera, E. Di Sipio, G. Cassiani, M. De Carli, A. Bernardi, An updated ground thermal properties database for GSHP applications, Geothermics 85 (2020) 101758.

[48] P. R. N. Hobbs, J. R. Hallam, A. Forster, D. C. Entwisle, L. D. Jones, A. C. Cripps, K. J. Northmore, S. J. Self, J. L. Meakin, Engineering geology of British rocks and soils Mudstones of the Mercia Mudstone Group, British Geological Survey Research Report (2002) 106 pp.

[49] D. Parkes, J. Busby, S. J. Kemp, E. Petitclerc, I. Mounteney, The thermal properties of the Mercia Mudstone Group Dan, Quarterly Journal of Engineering Geology and Hydrogeology (2020).

[50] A. S. Howard, G. Warrington, K. Ambrose, J. G. Rees, A formational framework for the Mercia Mudstone Group (Triassic) of England and Wales National Geoscience Framework Programme, British Geological Survey (2008).

[51] SimonHydrotechnica, Cardiff Dewatering Pilot Study: Final Report, Vol 1, Technical Report, SimonHydrotechnica, 1993.

[52] B. Williams, Cardiff Bay barrage: Management of groundwater issues, Proceedings of the Institution of Civil Engineers: Water Management 161 (2008) 313–321.

[53] Ordnance Survey Open Zoomstack, Contains OS data © crown copyright and database right, 2019.

[54] P. Bayer, J. A. Rivera, D. Schweizer, U. Schärli, P. Blum, L. Rybach, Extracting past atmospheric warming and urban heating effects from borehole temperature profiles, Geothermics 64 (2016) 289–299.

[55] A. Bidarmaghz, G. A. Narsilio, I. W. Johnston, S. Colls, The importance of surface air temperature fluctuations on long-term performance of vertical ground heat exchangers, Geomechanics for Energy and the Environment 6 (2016) 35–44.

[56] COMSOL Multiphysics® v. 5.6, Heat transfer module and subsurface flow module user's guide [online], 2020.

[57] D. Wilcox, Turbulence Modeling for CFD, D C W Industries, 3rd edition, 2006.

[58] G. R. Beardsmore, J. P. Cull, Heat Generation, in: Crustal Heat Flow, 2001, pp. 23–44.

[59] S. A. Baggs, Remote prediction of ground temperature in Australian soils and mapping its distribution, Solar Energy 30 (1983) 351–366.

[60] C. O. Popiel, J. Wojtkowiak, Temperature distributions of ground in the urban region of Poznan City, Experimental Thermal and Fluid Science 51 (2013) 135–148.

[61] NCAS British Atmospheric Data Centre, Met office integrated data archive system (midas) land and marine surface stations data (1853-current), 2020.

[62] B. M. A. Bernier, Closed-Loop Heat Pump Systems, Ashrae Journal (2006).

[63] M. Philippe, M. Bernier, P. Eng, D. Marchio, Vertical Geothermal Borefields, Ashrae Journal (2010) 10.

[64] G. R. Aditya, G. A. Narsilio, Environmental assessment of hybrid ground source heat pump systems, Geothermics 87 (2020) 101868.

[65] E. Ampatzi, I. Knight, Modelling the effect of realistic domestic energy demand profiles and internal gains on the predicted performance of solar thermal systems, Energy and Buildings 55 (2012) 285 – 298. Cool Roofs, Cool Pavements, Cool Cities, and Cool World.

Nikolas Makasis: Conceptualization, Formal analysis, Investigation; Methodology, Software, Writing - original draft

Monika J. Kreitmair: Conceptualization, Formal analysis, Investigation; Methodology, Visualization, Software, Writing - original draft

Asal Bidarmaghz: Conceptualization, Supervision, Validation, Writing - review & editing

Gareth J. Farr: Data curation, Investigation, Writing - review & editing

Johanna M. Scheidegger: Data curation, Investigation, Writing - review & editing

Ruchi Choudhary: Conceptualization, Funding acquisition, Project administration, Supervision, Writing - review & editing

Declaration of Interest Statement

Declaration of interests

☒ The authors declare that they have no known competing financial interests or personal relationships that could have appeared to influence the work reported in this paper.

☐The authors declare the following financial interests/personal relationships which may be considered as potential competing interests: